ACS APPLIED MATERIALS & INTERFACES

Research Article

www.acsami.org

Surfactant-Assisted Porphyrin Based Hierarchical Nano/Micro Assemblies and Their Efficient Photocatalytic Behavior

Sadananda Mandal,[†] Sandip K. Nayak,[‡] Sivaramakrishna Mallampalli,[§] and Amitava Patra*[,†]

[†]Department of Materials Science, Indian Association for the Cultivation of Science, Kolkata-700 032, India

[‡]Bio-organic Division, Bhabha Atomic Research Centre, Mumbai-400 085, India

[§]TDP, Heavy Water Board, Mumbai-400 094, India

Supporting Information

ABSTRACT: In this report, we have demonstrated the synthesis of surfactant-assisted different morphologies of *meso*-tetra(4-carboxyphenyl)porphyrin assemblies (spherical to flower shaped). These nano/micro assemblies are well characterized by scanning electron microscopy and X-ray diffraction. The formation of assemblies is driven by noncovalent interactions such as hydrophobic−hydrophobic and aromatic $\pi-\pi$ stacking between the molecules. The steady state and time-resolved spectroscopic investigation reveal that different assemblies are formed by virtue of special supramolecular organizations. The photocatalytic activities of different assemblies have been demonstrated with an organic pollutant Rhodamine B dye under the visible light irradiation. Such porphyrin based assemblies could pave the way for designing new optical based materials for the applications in photocatalytic, photovoltaic, and light harvesting system.

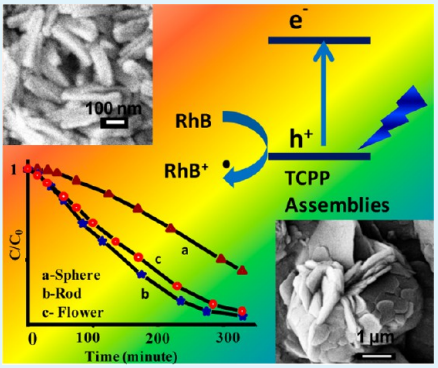

KEYWORDS: *porphyrin, assemblies, steady state, time-resolved spectroscopy, dye, photocatalysis*

INTRODUCTION

Inorganic and organic based self-assemblies have drawn a great attention owing to their unique optical as well as electronic properties for potential applications like catalysis, light energy conversion, optoelectronic devices, and biological sensors.[1−6] So far, numerous inorganic and organic based assemblies are intensively investigated. However, compared to the inorganic based assemblies, organic based assemblies have received a special attention owing to their solution processability and flexibility in molecular designing.[7−14] In particular, among the organic based self-assemblies, porphyrin and related compounds based assemblies are of great interest for versatile applications in sensing, light harvesting, and photocatalytics for their excellent photophysical, photochemical, electrochemical, and structural properties.[15−19] The porphyrinoid assembled structures have been synthesized by various methods. For example, Hasobe et al. has synthesized supramolecular nanorods of *meso*-diaryl-substituted porphyrin by a sonication method.[8] They have also synthesized nanocubes and microrods of *meso*-tetra(4-carboxyphenyl)porphyrin (TCPP) by a metal coordination-assisted mixed solvent method.[20] Aria and his co-workers have reported the synthesis of self-assembled nanostructures from zwitterionic *meso*-terakis-(sulfonatothienyl)porphyrin by changing the pH of the aqueous solutions.[21] Recently, Martin et al. have synthesized microscale four-leaf clover-shaped structures formed by self-assembly of anionic tin(IV) tetrakis(4-sulfonatophenyl)-porphyrin and cationic zinc(II) tetrakis(*N*-ethanol-4-pyridinium)porphyrin.[22] McHale and his co-workers have done extensive work on porphyrin based self-assembled structures for their potential use in light harvesting and solar cell systems.[23−27] Furthermore, surfactant-assisted nanospheres and nanorods of zinc *meso*-tetra(4-pyridyl)porphyrins have also been reported in a recent publication.[28] All of the preceding examples of supramolecular assembled structures are governed by the various noncovalent interactions, such as hydrogen bonding, $\pi-\pi$ stacking, hydrophobic, electrostatic interactions, and van der Waals forces, etc.[29−33] The (supra) molecular organizations are mainly J-type (offset-stack or steplike arrangement) and H-type (face-to-face arrangement) aggregates, which have unique electronic and spectroscopic properties due to their high structural order.[34,35] These organic assembled structures are found to be more attractive because of their good solubility, stability, and less toxicity compared to inorganic assembled structures.[36−39]

Herein, we have synthesized different morphologies of assembled structures (spherical, rods, flakes, and flowers) of *meso*-tetra(4-carboxyphenyl)porphyrin (TCPP) by a surfactant-assisted method using acid−base neutralization with varying stirring time. The morphologies of these assembled structures have been characterized by FESEM, XRD, and steady state and time-resolved spectroscopy. A plausible mechanism for the formation of well aggregated structures has been proposed. Furthermore, we have investigated the photocatalytic activity of

Received: August 21, 2013
Accepted: December 17, 2013
Published: December 17, 2013

Scheme 1. Molecular Structures of (A) TCPP and (B) Rhodamine B

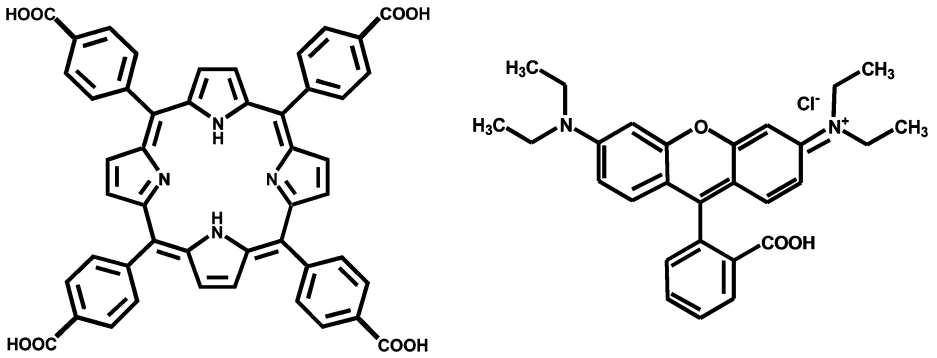

(A) (B)

these assembled structures with an organic pollutant RhB dye under the visible light irradiation. Rod shaped structures are found to be the most efficient photocatalytic activities. This high efficiency of photocatalytic activity in the porphyrin based assemblied structures opens up further prospects in potential applications as light-harvesting systems and other photodriven devices.

EXPERIMENTAL PROCEDURE AND CHARACTERIZATION

Materials. 4-Carboxybenzaldehyde (Sigma-Aldrich), propionic acid (Sigma-Aldrich), pyrrole (Sigma-Aldrich), cetyltrimethylammonium bromide (CTAB) [Alfa Aesar], sodium hydroxide (NaOH) [MECRK], hydrochloric acid (HCl) [MECRK], rhodamine B (RhB) [Sigma-Aldrich], tetrahydrofuran (THF) [MERCK], dichloromethane [MERCK], and deionized water [MERCK] were used as received. Molecular structures of TCPP and rhodamine B are depicted in Scheme 1.

Synthesis of 5,10,15,20-tetrakis(4-carboxyphenyl)porphyrin (TCPP). The synthesis of TCPP was reported previously.[40−42] Briefly, to a solution of 4-carboxybenzaldehyde (6.0 g, 0.04 mol) in hot propionic acid (400 mL) was added freshly distilled pyrrole (2.68 g, 2.8 mL, 0.04 mol) dropwise. The mixture was then refluxed for 45 min, cooled to ambient temperature, and kept in the refrigerator overnight. The dark solution was filtered and the brown solid was washed with dichloromethane. The crude solid was purified by column chromatography (silica, eluant $CHCl_3$−MeOH = 8:2) to get pure TCPP as a purple powder (0.180 g, 2.3%). The sample was well characterized by NMR, IR, and UV−vis studies. ^{1}H NMR (CD_3OD): δ 8.85 (bs, 8H, pyrrole β-H), 8.47 (d, J = 8.0 Hz, 8H), 8.28 (d, J = 8.1 Hz, 8H). IR: 3314, 2918, 1728, 1694, 1605, 794 cm^{-1}. UV−vis (λ_{max}): 415, 513, 547, 588, 645 nm.

Synthesis of Different Morphologies of Surfactant-Assisted TCPP Aggregates. Different morphologies of TCPP aggregates were synthesized by a typical acid−base neutralization strategy along with a hydrophobic interaction method. First, 0.004 g of TCPP was dissolved in 0.5 mL of 0.2 M NaOH solution. In another container, 0.0364 g of CTAB was dissolved in 9.5 mL of 0.0105 M HCl solution. Then, the TCPP solution was added to the CTAB containing solution with constant stirring (1200 rpm) at room temperature. The final concentration of TCPP was 0.5×10^{-3} M. The reaction was carried out in a 20 mL beaker covered with aluminum foil to avoid the photochemical reaction. Then 0.5 mL of this solution was taken out after 15 min, 1 h, 6 h, and 48 h to obtain different morphologies of surfactant-assisted TCPP aggregates. The samples are reproducible and stable for more than 15 days.

Characterization. Field emission scanning electron microscopy (FE-SEM, JEOL, JSM-6700F) was used to characterize different morphologies of TCPP aggregates. The crystallinity of the aggregates was identified by X-ray diffraction (XRD) using a Siemens model D 500, powder X-ray diffractometer using a Cu Kα source (1.5418 Å radiation). Room temperature optical absorption spectra were taken by a UV−vis spectrophotometer (SHIMADZU). Room temperature photoluminescence spectra were recorded by a Fluoromax-P (HORIBA JOBIN YVON) photoluminescence spectrophotometer. For the time correlated single photon counting (TCSPC) measurements, the samples were excited at 405 nm using a picosecond diode laser (IBH Nanoled-07) in an IBH Fluorocube apparatus. The typical full width at half-maximum (fwhm) of the system response using a liquid scatter was about 90 ps. The repetition rate was 1 MHz. The fluorescence decays were analyzed using IBH DAS6 software. The following equation was used to analyze the experimental time-resolved fluorescence decays, $P(t)$:[43]

$$P(t) = b + \sum_{i}^{n} \alpha_i \exp\left(-\frac{t}{\tau_i}\right) \quad (1)$$

Here, n is the number of discrete emissive species, b is a baseline correction ("dc" offset), and α_i and τ_i are the pre-exponential factors and excited-state fluorescence lifetimes associated with the ith component, respectively. For multiexponential decays the average lifetime, $\langle\tau\rangle$, was calculated from the following equation:[44]

$$\left\langle \tau \right\rangle = \sum_{i=1}^{n} a_i \tau_i \quad (2)$$

where $a_i = \alpha_i / \sum \alpha_i$ and a_i is contribution of the decay component. A xenon lamp (wavelength >400 nm) was used as visible light source to investigate the photocatalytic activity of the aggregated structures.

RESULTS AND DISCUSSION

1. Structural Investigation. Figure 1 shows the SEM images of different morphologies of surfactant-assisted TCPP at different stirring times. The spherical aggregates of porphyrin molecules with an average diameter of 100 nm are formed after 15 min of stirring. The spherical aggregates are transformed into rod shaped aggregates with the length of 230 and 73 nm width after 1 h of stirring. As the stirring time is extended to 6 h, flakes shaped microaggregates are formed. The average size of the flakes is 3.5 μm with 0.4−0.5 μm width. Finally, flower shaped aggregates are formed after 48 h of stirring and the average size of the flowers is about 4.5 μm.

What is (are) the driving force(s) for the formation of these different morphologies of TCPP aggregated structures? In general, TCPP molecules are insoluble in water. The carboxylic groups of TCPP are deprotonated in alkaline solution to form tetra-carboxylate anion, $[TCPP]^{-4}$, which is soluble in water.

dx.doi.org/10.1021/am403518d | ACS Appl. Mater. Interfaces 2014, 6, 130−136

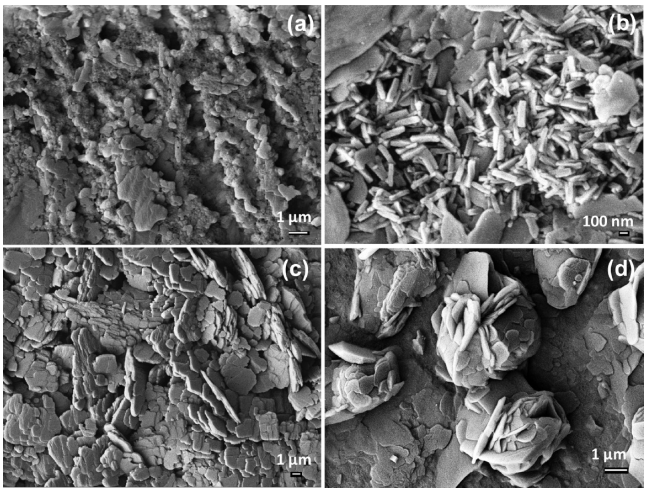

Figure 1. SEM images of surfactant-assisted different morphologies of TCPP aggregates (a) particles, (b) rods, (c) flakes, and (d) flowers.

The encapsulation process into the micelle occurs by adding this $[TCPP]^{-4}$ basic aqueous solution to acidic aqueous solution of surfactant (CTAB) under vigorous stirring. Here, the cationic surfactant CTAB might act as a stabilizer via the electrostatic interaction between the carboxylate anion in the porphyrin molecules and the cationic surfactant CTAB. Subsequently, the surfactant plays an important role on the formation of porphyrin aggregation. During acid−base neutralization, the $[TCPP]^{-4}$ anion becomes hydrophobic TCPPs after protonation. These hydrophobic TCPP molecules are encapsulated into the hydrophobic micelle because of the hydrophobic−hydrophobic interaction between porphyrin and CTAB molecules. When the stirring time is increased, the number of available porphyrin molecules in the micelle interior also increases, which might help to form different morphologies of TCPP aggregated structures, i.e. spherical, rods, flakes, and flowers. The formation of assembled structures is driven by the noncovalent interactions such as hydrophobic−hydrophobic and aromatic $\pi-\pi$ stacking between the molecules. A plausible mechanism is depicted in Scheme 2.

Control experiments have been done to understand the mechanism of formation of various morphologies of TCPP. Without adding surfactant (CTAB), the basic solution of $[TCPP]^{-4}$ is acidified by adding hydrochloric acid and their aggregation behavior is studied with different stirring times. Figure 2 shows the FE-SEM images of the TCPP aggregates at the different stirring times without surfactant. Fibril structures of porphyrin molecules are obtained just after 15 min of stirring. This fibril structures remain unchanged up to 1 h of stirring. These fibril structures started to break down after 6 h of stirring. Most of the fibres are broken into particles after 24 h of stirring. All fibres are broken into the particles after 48 h of stirring. Actually, the carboxylic groups of TCPP are deprotonated in NaOH(aq) solution and the tetra-carboxylate anion, $[TCPP]^{-4}$, forms a homogeneous solution. After acid−base neutralization, the $[TCPP]^{-4}$ anions become protonated to produce the insoluble TCPPs. The hydrophobic TCPP molecules are aggregated to form the fibril structures. As we increase the stirring time, the fibril structures try to form the small aggregates due to the lack of strong hydrophobic interactions. Finally, after 48 h, the fibril structures are broken into small particles. In the absence of any hydrophobic agent, small particles formation is thermodynamically more favorable

Scheme 2. Possible Mechanism of Surfactant-Assisted Different Morphologies of TCPP Aggregated Structures

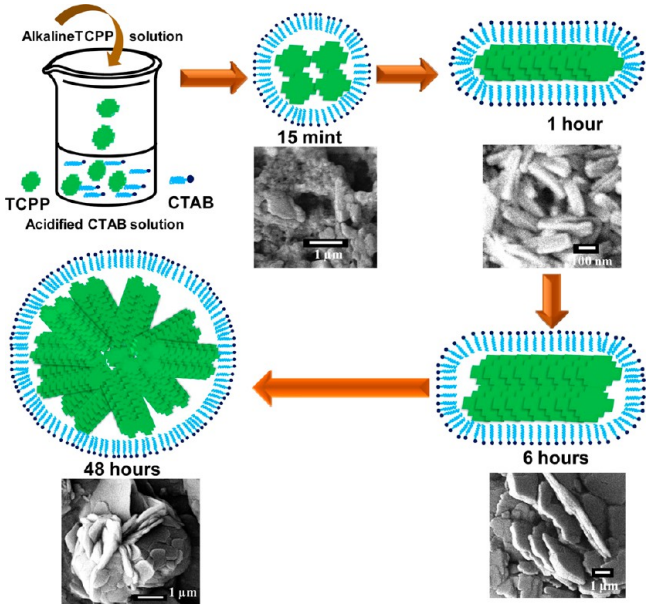

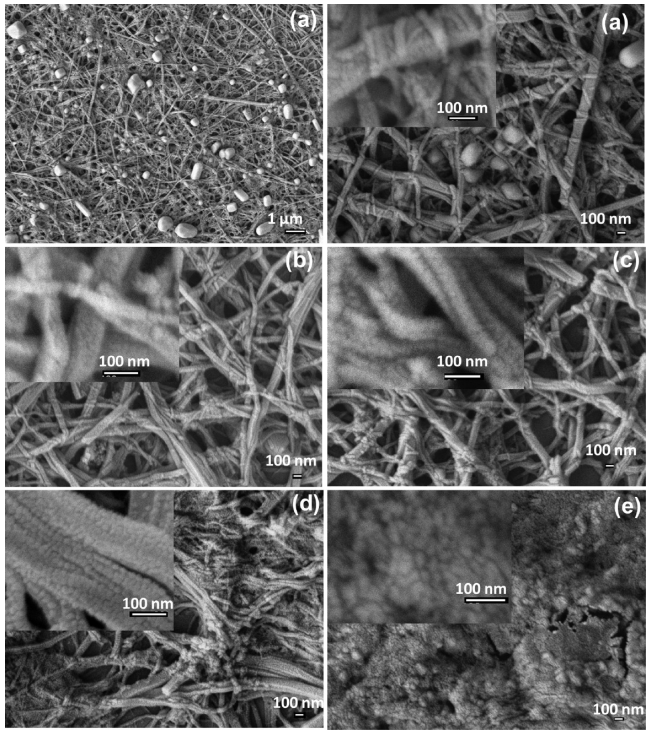

Figure 2. SEM images of different morphologies of TCPP without surfactant (a) 15 min, (b) 1 h, (c) 6, (d) 24, and (e) 48 h.

than the large assembly formation. It is important to note that the CTAB-assisted assembled structures are well dispersed in aqueous solution whereas the assembled structures without CTAB are not stable in aqueous solution. Thus, CTAB plays an important role in the formation of stable assembled structures of porphyrin molecule and morphology can be tuned by changing the stirring time.

Furthermore, the effects of concentration of porphyrin and pH of the systems at a particular stirring time (15 min) have been investigated. It is clearly seen from Figure 3 that the flake

dx.doi.org/10.1021/am403518d | ACS Appl. Mater. Interfaces 2014, 6, 130−136

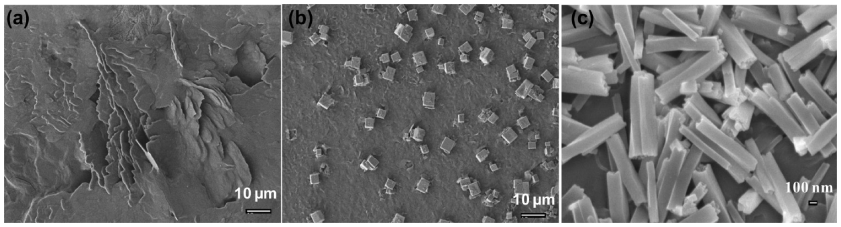

Figure 3. SEM images of the aggregated structures at stirring time 15 min (a) TCPP concentration 0.125×10^{-3} M, (b) TCPP concentration 0.5×10^{-3} M, pH 11.5, and (c) TCPP concentration 0.5×10^{-3} M, pH 2.0.

structures are formed at a 0.125×10^{-3} M concentration of porphyrin. The porphyrin molecules are aggregated to form cubic structures at pH 11.5 and a 0.5×10^{-3} M concentration of porphyrin. Keeping the same concentration of porphyrin (0.5×10^{-3} M), we observed the formation of rod shaped aggregates at pH 2.0. Thus, the cubic structure changes to rod shaped structure with changing the pH from 11.5 to 2.0. Therefore, the concentration of porphyrin and the pH of the system play an important role in the formation of self-assembled structures. We are now investigating the influence of concentration, pH, and other parameters on the formation of porphyrin assembled structures and their photocatalytic applications.

The internal structures of the surfactant-assisted different morphologies of TCPP aggregated structures are investigated by XRD analysis. Figure 4 depicts the XRD patterns of TCPP

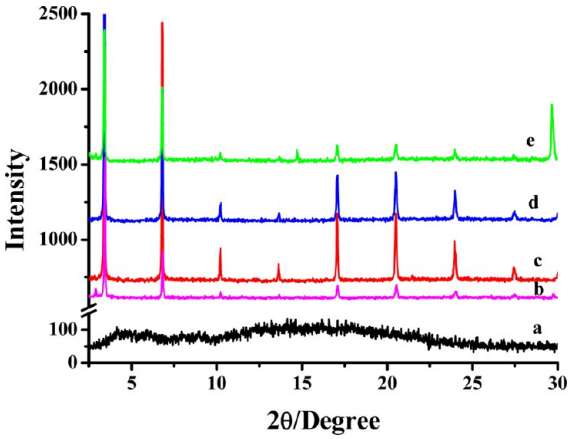

Figure 4. XRD of surfactant-assisted different morphologies of TCPP aggregates (a) monomer, (b) spherical, (c) rod, (d) flake, and (e) flower.

molecule and different aggregated structures (spherical, rod, flake, and flower shaped) of TCPP molecules. No refraction peak is observed for TCPP molecules, indicating the non-crystalline behavior of TCPP molecules. However, strong refraction peaks are observed in different morphologies of porphyrin aggregates, indicating the crystalline nature, which may be due to aromatic $\pi-\pi$ stacking between the porphyrin molecules.

2. Photophysical Properties of Assembled Structures. It is evident that porphyrin based assemblies have unique optical properties.[15,18,45] Porphyrins\metalloporphyrins exhibit a high-energy B band (known as Soret band) and low-energy Q bands. The Soret absorption band corresponds to S_0-S_2 electronic transitions, whereas Q-band corresponds to S_0-S_1 electronic transitions.[45] Both B and Q bands arise from $\pi-\pi^*$ electronic transitions. Thus, steady state and time-resolved spectroscopic studies have been performed to understand the photophysical properties of these assembled structures. Figure 5 shows the UV−vis spectra of different aggregates of TCPP

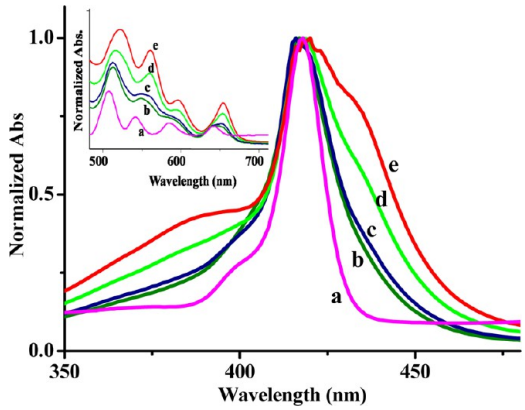

Figure 5. Absorption spectra (Soret band) of surfactant-assisted different morphologies of TCPP aggregates. Inset shows the corresponding Q band (a) monomer, (b) spherical, (c) rod, (d) flake, and (e) flower.

molecules. TCPP exists as monomer in THF solution and it exhibits a high intensity Soret band at 415 nm and four relatively weak Q bands at 513, 547, 588, and 645 nm. However, the Soret absorption band position slightly red-shifted with the spectral broadening in aggregated TCPP molecules. The calculated full widths at half-maxima (fwhm) are 12, 22, 23, 30, and 38 nm for the monomer, spherical, rod, flakes, and flower shaped aggregated TCPP, respectively. Broadening of the absorption spectra of aggregated species from the monomer unit implies the electronic interactions between porphyrin molecules due to their heterogeneity. The Q absorption bands are also red-shifted along with high absorbance with respect to TCPP monomer. These spectral characteristics imply the formation of porphyrin assemblies via J-type aggregation, which is consistent with the J-aggregation of zinc octaethylporphyrin in the polymer nanoparticle matrix.[18] Interestingly, both flake and flower shaped TCPP aggregates show a high energy band (as a shoulder) at the 380−390 nm range. The high energy band is due to the H-type aggregation of the porphyrin molecules, which is consistent with previous results.[46−48] To extract more information on the aggregation behavior of the porphyrin assembled structures, all the absorption spectra are deconvoluted by Gaussian distribution (depicted in Figure 6). The intensity of the peak at 415 nm gradually decreases from monomer to flower shaped assemblies. On the other hand, the intensity of the absorption bands at 395−405 nm and 420−430 nm is increased. McHale

dx.doi.org/10.1021/am403518d | ACS Appl. Mater. Interfaces 2014, 6, 130−136

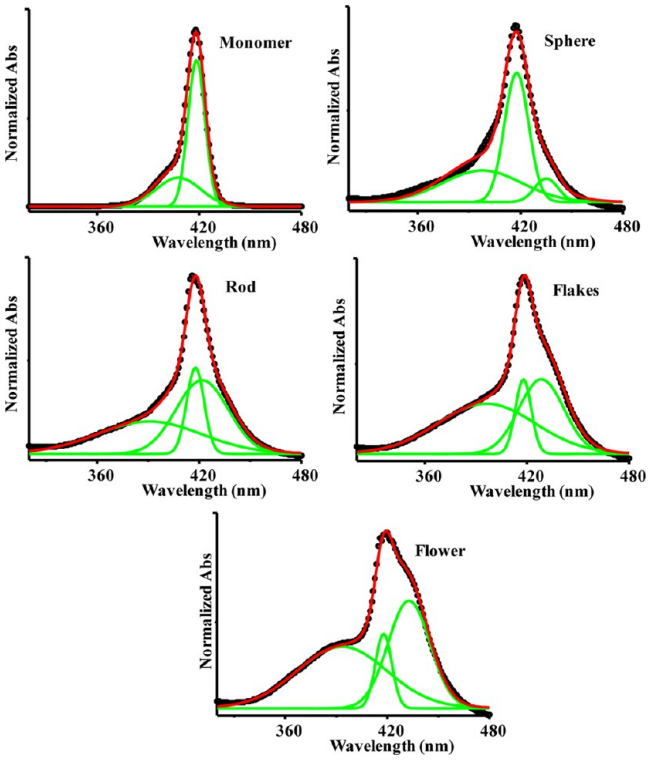

Figure 6. Deconvoluted absorption spectra (Soret band) of surfactant-assisted different morphologies of TCPP aggregates.

et.al[23,26] have also reported red-shifted (J band) and blue-shifted (H band) bands of TCPP aggregates. They have reported a doubly degenerated Soret band of TCPP aggregates due to orthogonal in plane transition dipoles. It is also reported that a single aggregate structure can give rise to both a blue-shifted and a red-shifted transition, which is different from the conventional J- and H-aggregation. They confirmed a single aggregated structure of TCPP aggregates by using resonance light scattering spectroscopy. In the present study, the TCPP aggregates may be formed by a single aggregate, but we could not confirm it due to the lack of the required instrumental facility.

Figure 7A shows the photoluminescence spectra and fluorescence decay curves of the corresponding TCPP aggregated structures. In THF solution, the TCPP monomer shows two emission bands, Q^*_{X00} and Q^*_{X01}, with maxima at 650 and 715 nm, respectively. This spectral pattern is a well-known characteristic of porphyrin molecules. When the TCPP molecules form aggregated structures, the maximum intense emission band becomes red-shifted with the spectral broadening. It is also observed that the red shifting and spectral broadening are increased more and more from spherical to flower shaped morphology. The low energy emission band becomes broadening after the formation of aggregated structures. The red shifting with spectral broadening of the emission spectra suggests the J-aggregation of porphyrin molecules.

For further information on the photophysical properties of porphyrin assemblies, the time-resolved fluorescence decays are measured at their corresponding emission wavelengths under a 405 nm excitation wavelength. Figure 7B shows the fluorescence decay of the TCPP monomer in THF, spherical, rod, and flower shaped TCPP aggregates. The decay curve of the TCPP monomer is fitted monoexponentially with the decay time of 11.10 ns. The other decay curves are fitted biexponentially. In the case of spherical assembled structures, the decay components are 1.78 and 5.54 ns and the average decay time is 2.56 ns. The decay components of rod shaped aggregates are 2.16 and 5.60 ns and the average decay time is 2.97 ns. In the case of flower shaped aggregates, the decay components are 2.73 and 8.24 ns and the average decay time is 4.17 ns. The shortening of decay time of TCPP aggregates from monomer, unambiguously confirms the J-type aggregation of the TCPP molecules. On the other hand, the increase of average decay time from 2.56 to 4.17 ns with changing from spherical aggregates to flower aggregates is an indication of partial H-type aggregation of TCPP molecules. The shortening of decay time of porphyrin molecules with respect to monomer and the enhancement of decay time of porphyrin molecules are because of the J- and H-aggregation of porphyrin, respectively.[46,48] Therefore, the time-resolved spectroscopic study further confirms the presence of J- and H- type aggregation in the flower shaped aggregated structures.

3. Photocatalytic Activity of Assembled Structures. The photocatalytic activities of TCPP aggregates of different morphologies are investigated with RhB dye under visible light irradiation. No photodegradation of RhB dye is observed in absence of either TCPP aggregates or visible light irradiation (Figures S1 and S2, Supporting Information). Thus, TCPP aggregates exhibit photocatalytic properties under the visible light irradiation only. Figures S3–S6 (Supporting Information) show the time dependent absorption spectra of the RhB in the

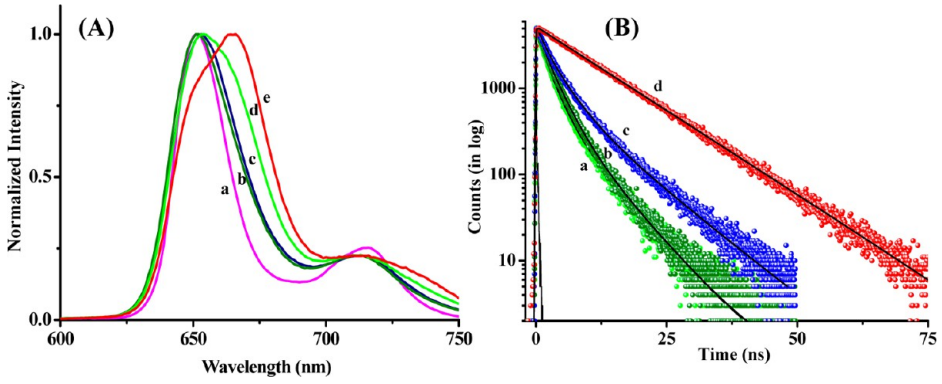

Figure 7. (A) Photoluminescence spectra (a) monomer, (b) spherical, (c) rod, (d) flake, and (e) flower; (B) photoluminescence decay curves (a) spherical, (b) rod, (c) flower, and (d) monomer.

dx.doi.org/10.1021/am403518d | ACS Appl. Mater. Interfaces 2014, 6, 130–136

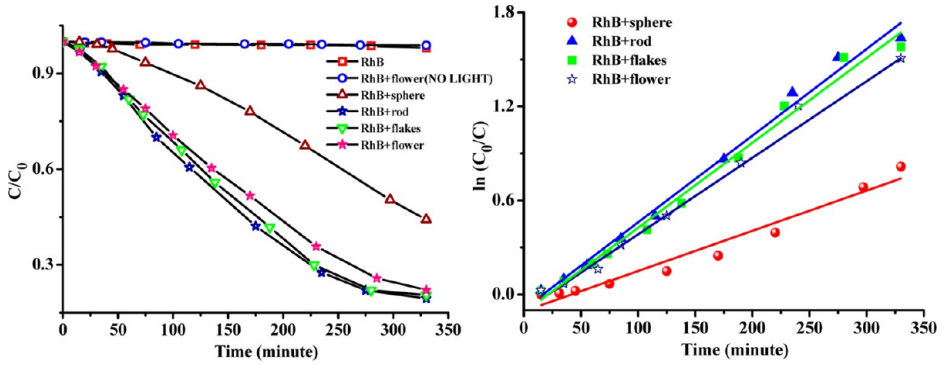

Figure 8. Photocatalytic activity of surfactant-assisted different morphologies of TCPP aggregates.

presence of different morphologies of TCPP aggregates under light irradiation. The decrease in the absorption peak (557 nm) of dye with time indicates the photocatalytic degradation of RhB.

The degradation rate can be calculated by using the following expression:

$$D\% = \frac{C_0 - C}{C_0} \times 100\% \quad (3)$$

where C_0 is the initial concentration of RhB and C is the concentration at time t. The calculated degradation rates of RhB are 56%, 81%, 79%, and 71% for the spherical, rod, flakes, and flower shaped TCPP aggregated structures, respectively. Figure 8 shows the C/C_0 versus time plot of RhB in the presence of different morphologies of TCPP aggregates. These observations clearly indicate that the photocatalytic activity depends upon the morphology of the TCPP aggregated structures. In case of J-aggregation of π-conjugated organic molecules, a strong intermolecular π electronic coupling occurs between the coherently aligned chromophores, which enhances the coherent electronic delocalization over the aggregated molecules due to the strong intermolecular $\pi-\pi$ interactions.[49,50] In the nonaggregated monomers, the π-conjugated electrons are locally delocalized over their macrocyclic plane, and hence a very weak intermolecular $\pi-\pi$ interaction occurs. Porphyrin monomers are not good photosemiconductors compared to J-aggregated porphyrin molecules.[50] A possible mechanism has been given to explain the results. In the case of spherical TCPP aggregates, most of the porphyrin molecules exist as monomeric species. They are in contact to each other by forming complexes with CTAB molecules. In case of rod shaped TCPP aggregates, the porphyrin molecules are cooperatively aligned as J-aggregates with a slipped cofacial arrangement. As a result, rod shaped aggregates have stronger intermolecular $\pi-\pi$ interactions than the spherical aggregates. The J-aggregated structures enhance the coherent electronic delocalization and become an efficient photosemiconductor. Recently, Guo et al. also reported that nanofibers have more photocatalytic efficiency than the spherical nano aggregates of ZnTPyP.[39] Similarly, the photocatalytic activities of the TCPP based flakes and flowers are less efficient than that of rod shaped TCPP aggregates. It is evident from spectroscopic data that the porphyrin molecules are in both J- and H-aggregations in flakes and flower shaped aggregates. It is proposed that J-aggregates exhibit more photocatalytic efficiency due to the coherent electronic delocalization which could facilitate the electron transfer process.[35,39] However, the H-aggregated molecules may diminish the intermolecular $\pi-\pi$ interactions in the flake and flower shaped aggregates. As a result, the photocatalytic efficiency of the flakes and flower shaped aggregates is lower than rod shaped TCPP aggregates.

CONCLUSION

In summary, we have successfully synthesized different surfactant-assisted assembled structures (spherical to flower shaped) of TCPP by varying the stirring time. The morphology of the assembled structures is well characterized by SEM and XRD. Steady state and time-resolved spectroscopic studies reveal the unique photophysical properties of the assembled structures and confirm the J-type aggregation of the porphyrin molecules. These assembled structures, specifically rod shaped aggregates, exhibit efficient photocatalytic activity (81%) under visible light irradiation. This study undoubtedly demonstrates that the porphyrin based assemblies could pave the way for developing new challenging photonic devices.

ASSOCIATED CONTENT

Supporting Information

Figure S1 shows the absorption spectra of RhB in absence of TCPP aggregates under visible light irradiation. Figure S2 shows the absorption spectra of RhB in presence of rod shaped TCPP aggregates without visible light irradiation. Figure S3 shows absorption spectra of RhB in presence of spherical TCPP aggregates under visible light irradiation. Figure S4 shows absorption spectra of RhB in presence of rod shaped TCPP aggregates under visible light irradiation. Figure S5 shows absorption spectra of RhB in presence of flake shaped TCPP aggregates under visible light irradiation. Figure S6 shows absorption spectra of RhB in presence of flower shaped TCPP aggregates under visible light irradiation. This material is available free of charge via the Internet at http://pubs.acs.org.

AUTHOR INFORMATION

Corresponding Author

*A. Patra. E-mail: msap@iacs.res.in. Phone: (91)-33-2473-4971. Fax: (91)-33-2473-280.

Notes

The authors declare no competing financial interest.

ACKNOWLEDGMENTS

"DAE-SRC Outstanding Investigator Award" is gratefully acknowledged for financial support. S.M. thanks CSIR for awarding fellowship.

REFERENCES

(1) Lehn, J.-M. *Science* **2002**, *295*, 2400−2403.
(2) Xiao, J.; Qi, L. *Nanoscale* **2011**, *3*, 1383−1396.
(3) Lin, C.; Zhu, W.; Yang, H.; An, Q.; Tao, C.-a.; Li, W.; Cui, J.; Li, Z.; Li, G. *Angew. Chem., Int. Ed.* **2011**, *50*, 4947−4951.
(4) Jang, J.; Oh, J. H. *Adv. Mater.* **2003**, *15*, 977−980.
(5) Qi, L . *Coord. Chem. Rev.* **2010**, *254*, 1054−1071.
(6) Ding, Q.; Miao, Y.-E.; Liu, T. *ACS Appl. Mater. Interfaces* **2013**, *5*, 5617−5622.
(7) Gong, X.; Milic, T.; Xu, C.; Batteas, J. D.; Drain, C. M. *J. Am. Chem. Soc.* **2002**, *124*, 14290−14291.
(8) Hasobe, T.; Oki, H.; Sandanayaka, A. S. D.; Murata, H. *Chem. Commun.* **2008**, *6*, 724−726.
(9) Hasobe, T.; Imahori, H.; Fukuzumi, S.; Kamat, P. V. *J. Mater. Chem.* **2003**, *13*, 2515−2520.
(10) Lee, S. J.; Hupp, J. T.; Nguyen, S. T. *J. Am. Chem. Soc.* **2008**, *130*, 9632−9633.
(11) Yan, Y.; Lin, Y.; Qiao, Y.; Huang, J. *Soft Matter* **2011**, *7*, 6385−6398.
(12) Drain, C. M.; Varotto, A.; Radivojevic, I. *Chem. Rev.* **2009**, *109*, 1630−1658.
(13) Jiang, L.; Fu, Y.; Li, H.; Hu, W. *J. Am. Chem. Soc.* **2008**, *130*, 3937−3941.
(14) Frühbeißer, S.; Gröhn, F. *J. Am. Chem. Soc.* **2012**, *134*, 14267−14270.
(15) *The Porphyrin Handbook*, Vol. *6*, Kadish, K. M., Smith, K. M., Guilard, R., Eds.; Academic Press: San Diego, CA, 2000; Vol. *6*, p 346.
(16) Schwab, A. D.; Smith, D. E.; Bond-Watts, B.; Johnston, D. E.; Hone, J.; Johnson, A. T.; De Paula, J. C.; Smith, W. F. *Nano Lett.* **2004**, *4*, 1261−1265.
(17) Mandal, S.; Bhattacharyya, S.; Borovkov, V.; Patra, A. *J. Phys. Chem. C* **2011**, *115*, 24029−24036.
(18) Mandal, S.; Bhattacharyya, S.; Borovkov, V.; Patra, A. *J. Phys. Chem. C* **2012**, *116*, 11401−11407.
(19) Arai, T.; Tanaka, M.; Kawakami, H. *ACS Appl. Mater. Interfaces* **2012**, *4*, 5453−5457.
(20) Sakuma, T.; Sakai, H.; Hasobe, T. *Chem. Commun.* **2012**, *48*, 4441−4443.
(21) Arai, Y.; Segawa, H. *Chem. Commun.* **2010**, *46*, 4279−4281.
(22) Martin, K. E.; Wang, Z.; Busani, T.; Garcia, R. M.; Chen, Z.; Jiang, Y.; Song, Y.; Jacobsen, J. L.; Vu, T. T.; Schore, N. E.; Swartzentruber, B. S.; Medforth, C. J.; Shelnutt, J. A. *J. Am. Chem. Soc.* **2010**, *132*, 8194−8201.
(23) McHale, J. L. *J. Phys. Chem. Lett.* **2012**, *3*, 587−597.
(24) Friesen, B. A.; Wiggins, B.; McHale, J. L.; Mazur, U.; Hipps, K. W. *J. Phys. Chem. C* **2011**, *115*, 3990−3999.
(25) Doan, S. C.; Shanmugham, S.; Aston, D. E.; McHale, J. L. *J. Am. Chem. Soc.* **2005**, *127*, 5885−5892.
(26) Choi, M. Y.; Pollard, J. A.; Webb, M. A.; McHale, J. L. *J. Am. Chem. Soc.* **2003**, *125*, 810−820.
(27) Friesen, B. A.; Wiggins, B.; McHale, J. L.; Mazur, U.; Hipps, K. W. *J. Am. Chem. Soc.* **2010**, *132*, 8554−8556.
(28) Bai, F.; Sun, Z.; Wu, H.; Haddad, R. E.; Coker, E. N.; Huang, J. Y.; Rodriguez, M. A.; Fan, H. *Nano Lett.* **2011**, *11*, 5196−5200.
(29) Ikeda, M.; Takeuchi, M.; Shinkai, S. *Chem. Commun.* **2003**, *12*, 1354−1355.
(30) Estroff, L. A.; Hamilton, A. D. *Chem. Rev.* **2004**, *104*, 1201−1217.
(31) Ryu, J.-H.; Lee, M. *J. Am. Chem. Soc.* **2005**, *127*, 14170−14171.
(32) Lee, E.; Kim, J.-K.; Lee, M. *Angew. Chem., Int. Ed.* **2008**, *47*, 6375−6378.
(33) Chen, L.; Revel, S.; Morris, K.; Adams, D. J. *Chem. Commun.* **2010**, *46*, 4267−4269.
(34) Kasha, M. *Radiat. Res.* **1963**, *20*, 55−70.
(35) Kano, H.; Kobayashi, T. *J. Chem. Phys.* **2002**, *116*, 184−195.
(36) Marin, M. L.; Santos-Juanes, L.; Arques, A.; Amat, A. M.; Miranda, M. A. *Chem. Rev.* **2012**, *112*, 1710−1750.
(37) Liu, H.; Feng, W.; Kee, C. W.; Zhao, Y.; Leow, D.; Pan, Y.; Tan, C.-H. *Green Chem.* **2010**, *12*, 953−956.
(38) Neumann, M.; Fueldner, S.; Koenig, B.; Zeitler, K. *Angew. Chem., Int. Ed.* **2011**, *50*, 951−954.
(39) Guo, P.; Chen, P.; Ma, W.; Liu, M. *J. Mater. Chem.* **2012**, *22*, 20243−20249.
(40) Datta-Gupta, N.; Bardos, T. J. *J. Heterocycl. Chem.* **1966**, *3*, 495−502.
(41) Kosal, M. E.; Chou, J.-H.; Suslick, K. S. *J. Porphyrins Phthalocyanines* **2002**, *6*, 377−381.
(42) Benedito, F. L.; Nakagaki, S.; Saczk, A. A.; Peralta-Zamora, P. G.; Costa, C. M. M. *Appl. Catal., A* **2003**, *250*, 1−11.
(43) Lakowicz, J. R. *Principles of Fluorescence Spectroscopy*, 3rd ed.; Kluwer Academic/Plenum Publishers: New York, 1999; p 496.
(44) Mandal, S.; Rahaman, M.; Sadhu, S.; Nayak, S. K.; Patra, A. *J. Phys. Chem. C* **2013**, *117*, 3069−3077.
(45) *Porphyrins and Metalloporphyrins*, Smith, K. M., Ed; Elsevier: Amsterdam, 1975; p 910.
(46) Maiti, N. C.; Mazumdar, S.; Periasamy, N. *J. Phys. Chem. B* **1998**, *102*, 1528−1538.
(47) Choi, M.-S. *Tetrahedron Lett.* **2008**, *49*, 7050−7053.
(48) Verma, S.; Ghosh, A.; Das, A.; Ghosh, H. N. *J. Phys. Chem. B* **2010**, *114*, 8327−8334.
(49) Satake, A.; Kobuke, Y. *Org. Biomol. Chem.* **2007**, *5*, 1679−1691.
(50) Wuerthner, F.; Kaiser, T. E.; Saha-Moeller, C. R. *Angew. Chem., Int. Ed.* **2011**, *50*, 3376−3410.